

Information Assisted Dictionary Learning for fMRI data analysis.

Manuel Morante^{a,b}, Yannis Kopsinis^{c,b}, Sergios Theodoridis^{d,a,b}

^a*Dept. of Informatics and Telecommunications, University of Athens (Greece)*

^b*Computer Technology Institute & Press “Diophantus” (CTI), Patras (Greece)*

^c*LIBRA MLI Ltd, Edinburgh (UK)*

^d*IAASARS, National Observatory of Athens, GR-15236, Penteli (Greece)*

Abstract

Extracting information from functional magnetic resonance images (fMRI) has been a major area of research for many years, but is still demanding more accurate techniques. Nowadays, we have a plenty of available information about the brain-behavior that can be used to develop more precise methods. Thus, this paper presents a new Dictionary Learning method that allows incorporating external information regarding the studied problem, through a novel sets of constraints. Finally, we apply this proposed method to synthetic fMRI data, where several tests show an improvement in the performance compared with other common techniques.

Keywords: fMRI, semi-blind, Dictionary Learning, sparsity, weighted norms

1. Introduction

Functional Magnetic Resonance Imaging (fMRI) is a powerful non-invasive technique for localizing and analyzing brain activity [1]. Studying the different areas within the brain that are associated with important tasks such as vision, perception, etc., constitutes a major area of research that demands robust and high precision techniques for the analysis of fMRI data [2], [3], [4].

Performing various human actions, as mentioned before, lead to the simultaneous activation of a number of *functional brain networks* (FBN), which are engaged in proper interactions to effectively execute the task. Such networks are usually related to low-level brain functions and they are defined as a number of *segregated* specialized small brain regions, potentially distributed over the whole brain. These regions collaborate in order to coherently perform a specific brain function. For each FBN, the segregated brain regions involved define a *spatial map*. Moreover, these brain regions, irrespective of their anatomical proximity or remoteness, exhibit a strong functional connectivity. This can be quantified via measuring the underlying correlation between the corresponding activation/deactivation time-patterns, referred to as *time courses*. Examples of

such brain networks are the visual, sensorimotor, auditory, default-mode, dorsal attention, and executive control networks.

Most commonly, fMRI is based on blood oxygenation level-dependent (BOLD) contrast, which essentially measures the local changes in the level of oxygen caused by the neuronal activity. This is achieved by exploiting the different magnetic properties of oxygen-saturated versus oxygen-desaturated hemoglobin. Accordingly, the time courses rather than being the actual neuronal activation patterns of the involved FBNs are the evoked hemodynamic response of the brain to this neuronal activity. This process is modeled as the convolution between the actual neuronal activation and a *person-dependent* impulse response function called Hemodynamic Response Function (HRF).

The obtained fMRI measurements associated to each voxel, comprise a mixture of the time courses of all the FBNs, which are active in the corresponding voxels. Moreover, beyond the aforementioned brain-induced sources that are contributing to the measured mixture, a number of machine-induced interfering sources are also present. The aim of fMRI data analysis is to unmix the measured mixture in order to reveal brain-induced time courses of interest and the associated spatial maps.

In any experimental fMRI design, there are two common activation schemes: the *block* paradigm and the *event-related* paradigm [5]. In the block paradigm, the subject is presented with a number of specified stimuli, usually two or three, referred to as *conditions*. Typical examples comprise a set of different images or an image appearing in different places or different colors, patterns, categories, etc. The conditions appear repetitively in a certain order and each one of them occupies pre-specified time frames of fixed duration. Moreover, the subject might be asked to perform an action, e.g., to press a switch to signal positive or negative feedback as a response. In the event-related experimental design paradigm, the conditions appear in a random order and for random time durations, which are usually shorter than those in the block design. Brain areas of high activation and correlation to the stimulation/response pattern are considered as highly relevant to the specific functional task (visual/motor centers, pain receptors, etc). A challenging fMRI experimental procedure is the task-free one, referred to as *resting-state* fMRI. In this case, there is no correlation to previously known activation patterns, induced by external stimulus to the subject; the functional analysis of the brain activity needs to be realized fully blindly.

One way to proceed the analysis of the fMRI data, in the case of block design or event-related experimental design, is to estimate the shape of the time-courses that correspond to the externally imposed experimental activation set up. Such time-courses are hereafter referred to as *task-related time courses*. Conventional analysis of fMRI data heavily rely on approaches focused on the General Lineal Model (GLM), which is based on prior availability of the task-related time courses [6]. After fitting the model in each voxel independently, statistical testing is performed in order to detect those voxels that are activated by each task-related time course or linear combinations of them. Moreover, visualisations of the voxels' activation level is achieved via statistical parameter

mapping (SPM), where active voxels are color-coded according to their p-values (or other comparable statistics) [7]. The GLM/SPM framework and its variants are implemented in the SPM software [8], which has arguably become the dominant tool to analyse fMRI data. Nevertheless, the aforementioned approach suffers from several limitations. The most prominent among them are: a) It assumes that the HRF function is known; although the HRF varies significantly across different persons as well as across different areas of the same brain [9], in practice, an assumption need to be made. b) The hypothesis testing on whether a voxel is active due to the experimental task or not, requires the proper tuning of a threshold, which ensures statistical significance. However, the setup of this critical threshold is tricky and it is often the source of systematic errors and misinterpretations [10].

An alternative route to fMRI data analysis is via the Blind Source Separation (BSS) method performed via a matrix factorization scheme. In general, matrix factorization methods are flexible approaches to unravel the involved latent factors via, for example, low-rank or sparse modeling techniques. Moreover, such methods are robust enough to accommodate externally imposed sets of constraints and have gained significant attention in several applications beyond fMRI [2]. BSS methods aim at alleviating some of the limitations that the classical GLM/SPM approach suffers from. For example, they do not adopt any assumption regarding the HRF, they inherently model interfering artifacts, such as machine-induced artifacts or uncorrected head-motion residuals that may obscure the brain activity of interest, and they can discover brain-induced sources beyond the task-related ones. Hence, they can also be applied on resting state fMRI experimental tasks and they can support several strategies for joint analysis of multi-sessions and multi-subjects datasets.

However, a blind matrix factorization task does not lead to a unique solution, and the results depend on the specific imposed constraints. Based on such constraints, two are the major techniques adopted for fMRI data analysis: Independent Component Analysis (ICA) and Dictionary Learning (DL).

ICA can be seen as a matrix factorization approach, which imposes the assumption of independence in different ways. This method has been used in fMRI data for solving the unmixing problem for many years [11] and it is still an active field of research [12]. Nevertheless, although ICA has been widely applied for fMRI analysis, due to its capability to separate spatially or temporally independent components, it has been observed by several authors that there exist certain situations where the independence hypothesis is seriously violated [13], [14]. Moreover, and more important, there is not any physical evidence to justify that sources are necessarily independent; the independence hypothesis has been strongly challenged, in particular in the context of resting state fMRI [15].

On the other hand, DL approaches are built around sparsity-related assumptions. Although sparsity is a natural assumption underlying the fMRI data generation, standard sparsity-aware learning methods still have several drawbacks that should be taken in to consideration. The most remarkable is that most of the DL methods require the selection of a regularization parameters

that control the “sparsity level” [2], [16], [17], [18]. Such as user defined parameters lack of a direct physical interpretation and are artificially introduced by the optimization process; this implies that their selection depends on the specific data set and relies on cross-validation argument. Nevertheless, cross-validation arguments has no practical meaning when working with fMRI real data.

Another less obvious –but decisive– drawback is that most of the sparsity constraints are unnaturally set: in real fMRI data each brain-like source is expected to be sparse, but most of the DL method consider sparsity constraints following other structures rather than is a proper source by source basics. Consequently, all these bad-conditioned constraints can lead to inconsistent results, making DL unsuitable for real fMRI data. Thus, in this paper, we present a variant of the ℓ_1 -norm constraint, which promotes sparsity in a natural way and alleviates these two aforementioned drawbacks.

Despite the numerous interesting characteristics that the matrix factorization approaches have, they are still not the first line approaches for task-fMRI analysis. The reason for that is a critical weakness that they exhibit against GLM/SPM approach; when two or more task-related sources manifest themselves in highly overlapped brain regions, then all BSS methods, to a larger (ICA) or smaller (DL) degree, can fail to discriminate them. This situation is common in numerous experimental designs of interest in which the different experimental conditions can activate the same major functional brain network, e.g., the auditory, the visual etc. On the contrary, SPM provides the option to study the contrast among different conditions, aiming at detecting brain areas which are explicitly activated due to a specific task.

The enhanced discriminative power of SPM comes from the fact that the time-course related information corresponding to each experimental condition is explicitly incorporated into the GLM modeling via the estimated BOLD sequences. Such information is left unexploited in the BSS framework. Hence, in order to fully exploit the power and merits of matrix factorisation-based methods, it is imminent need to be able to effectively enhance the source unmixing by exploiting the aforementioned time-courses; this would render the whole decomposition process to be semi-blind rather than fully blind.

With respect to ICA, semi-blind techniques have been adopted in an attempt to embed prior knowledge into the associated estimation task [19]. Unfortunately, the independence hypothesis is very restrictive and still limits all these approaches, as the standard ICA. Consequently, semi-blind ICA methods require a special care when task-related time courses are involved, because they may elicit largely overlapping responses with other sources or even other imposed task-related time courses [10] that strongly violates the independence assumptions [20]. For this reason, when external information is imposed, it is needed to analyze how the imposed task-related time courses affect the rest of the sources, which is impossible to predict in practice, since the sources are a priori unknown.

On the other hand, DL-based methods can adopt any prior information in the form of constraint, since sparsity is the only underlying assumption. In fact, a method called *Supervised Dictionary Learning* (SDL) [21] allows the in-

corporation of external information from the task-related time courses similarly to GLM. Thus, SDL paves the way to new directions of research in fMRI, as well as for other applications, like Hyperespectral imaging, where, also, semi-blind ICA-based methods can not be implemented due to the independence hypothesis [22]. However, the SDL method still shares the same drawbacks as the GLM: the imposed time courses are assumed to be known using a predefined functional form for the HRF, which is considered fixed over the whole brain and from subject to subject. This is a strong and unrealistic hypothesis, which also compromises a major advantage of BSS methods for fMRI analysis; that is, they are not restricted by HRF assumptions, that are deemed to be wrong in a larger or smaller degree. In this paper, the DL approach has been appropriately reformulated in order to allow the incorporation of *weak constraints* associated to any time-course; thus, the unmixed sources are not restricted to fully comply with the imposed time-courses but they are only encouraged to be similar.

Major Contributions

The major contributions of this paper are summarized as follows:

- We propose a new semi-blind DL approach that incorporates a priori knowledge relate to the *approximate* shape of the whole task-related time courses. This approach enhances the discrimination power of the DL method, especially, in separate overlapped experimental conditions, but it also account for the fact that our knowledge about the HRF is deemed to be relatively inaccurate or even dynamically changing.
- We introduce a new sparsity constraint based on the weighted ℓ_1 -norm, which explicitly incorporates sparsity information in a thoughtful way and bypasses the need of introducing unnatural regularization parameters. Instead, the new constraints are associate with a physical meaning and facilitates the way that Neuro-scientist can include information related to the area occupancy of different functional brain networks, which are expected to be detected, exploiting, e.g., info documented in defined brain atlases [23].
- The new proposed sparsity constraint is more flexible and can consider the existence of non-sparse sources (dense). In real fMRI, some of the sources can be dense, which are related to certain machine artifacts.
- The new proposed method offers a proper alternative to other standard DL methods that promotes sparsity on a voxel by voxel basis [16]. Instead, the proposed DL method incorporates sparsity in a source by source basis; explicitly handling the sparsity of each spatial map and naturally complying with the physical interpretation of the segregated functional brain networks.
- We provide a realistic synthetic data set, which is used to study the efficiency of the proposed method and to compare its performance with

other standard DL methods. Although results with real data have been obtained, in this paper we will only report simulated experiments.

Notation

Scalars are denoted by lower case letters, x , a bold capital letter, \mathbf{X} , denotes a matrix and a bold lower case letter, \mathbf{x} , denotes a vector with its i^{th} component denote as x_i . The i^{th} row and the i^{th} column of a matrix $\mathbf{X} \in \mathbb{R}^{M \times N}$, are denoted as $\mathbf{x}^i \in \mathbb{R}^{1 \times N}$ and $\mathbf{x}_i \in \mathbb{R}^{M \times 1}$, respectively. Moreover, x_{ij} denotes the element found in row i and column j of matrix \mathbf{X} .

Given an arbitrary vector, $\mathbf{w} \in \mathbb{R}^N$, the notation $\mathbf{w} > a$ stands for $w_i > a \forall i = 1, 2, \dots, N$.

The vector $\mathbf{1}_N$ denotes a column vector of size N having all components equal to one and \mathbf{I}_N is the identity matrix of size $N \times N$. Furthermore, $\mathbf{A} = \text{diag}(\mathbf{x})$ is a diagonal matrix having $a_{ii} = x_i$.

2. Problem Statement

During the course of a task-related fMRI experiment, a sequence of 3D images of the brain are successively acquired along time, while the subject performs a set of predetermined tasks according to the chosen experimental design. Each one of these 3D images is formed by a grid of elementary volume units called *voxels*. These voxels can be thought of as cubes, which define the smallest measurable volume of a brain tissue. Accordingly, the signal detected at each voxel reflects the degree of activity of the set of neurons contained in the corresponding small volume [1].

Each 3D image is unfolded and stored in a vector, $\mathbf{x} = [x_1, x_2, \dots, x_N]^T \in \mathbb{R}^{1 \times N}$, where N is the total number of voxels per image. The vectors corresponding to the sequence of, say T , acquired images are concatenated as rows in the data matrix $\mathbf{X} \in \mathbb{R}^{T \times N}$.

Note that, in practice, prior to the formation of the data matrix, \mathbf{X} , several standardized preprocessing steps are conducted in order to account for a number of detrimental effects related to the fMRI image acquisition process, such as slice timing correction, head motion, realignment normalization, etc.

From a mathematical point of view, the source separation problem can be described as a matrix factorization task of the data matrix, i.e.,

$$\mathbf{X} \approx \mathbf{D}\mathbf{S}, \tag{1}$$

where, following the dictionary learning jargon, $\mathbf{D} \in \mathbb{R}^{T \times K}$ is the dictionary matrix, whose columns represent the time courses, $\mathbf{S} \in \mathbb{R}^{K \times N}$, is the coefficient matrix, whose rows represent the spacial maps associated with the corresponding time courses and K is the number of sources.

In general, this matrix factorization can be expressed as a constrained optimization task given by:

$$(\hat{\mathbf{D}}, \hat{\mathbf{S}}) = \underset{\mathbf{D}, \mathbf{S}}{\text{argmin}} \|\mathbf{X} - \mathbf{D}\mathbf{S}\|_F^2 \quad \text{s.t.} \quad \begin{matrix} \mathbf{D} \in \mathfrak{D} \\ \mathbf{S} \in \mathfrak{L} \end{matrix}, \tag{2}$$

where \mathbf{X} is the data matrix and \mathfrak{D} , \mathfrak{L} are two sets of admissible matrices, defined via the set of the imposed constraints.

2.1. Sparse Approximation

The concept of sparsity refers to the number of zero-values that a digital signal has. In numerous applications, sparsity is the cornerstone of several systems whose response can be modeled using a small number of non-zero coefficients. In the fMRI framework, sparsity can suitably model the segregated nature of the spatial maps. In particular, each row of the coefficient matrix, \mathbf{S} , should have non-zero values at the entries that correspond to voxels activated by the corresponding time course, only.

No doubt, the best way to measure sparsity is using the ℓ_0 -norm. Formally, given an arbitrary vector $\mathbf{x} \in \mathbb{R}^N$, the ℓ_0 -norm (which strictly speaking is not a true norm) can be defined as the cardinality of the support of the vector \mathbf{x} :

$$\|\mathbf{x}\|_0 = \#\text{supp}(\mathbf{x}), \quad (3)$$

where $\text{supp}(\mathbf{x}) = \{i \in [1, N] \mid x_i \neq 0\}$ is the support of the vector \mathbf{x} . In other words, the ℓ_0 -norm is equal to the number of non-zero components of a vector.

Observe that the ℓ_0 -norm depends on the size of the vector. For this reason, sometimes, it is more convenient to use the *proportion of zero values* of a vector, often called *level of sparsity* [24]. For example, given an arbitrary vector $\mathbf{x} \in \mathbb{R}^N$, then its level of sparsity is given by:

$$l = 1 - \frac{\|\mathbf{x}\|_0}{N}, \quad (4)$$

where N is the total number of elements of the vector \mathbf{x} , and $l \in [0, 1]$ is the proportion of non-zero values. Sometimes, the level of sparsity is more convenient; since it simultaneously consider the number of non-zero values and the size of the vector, which makes its use more intuitive.

The matrix factorization framework that explicitly exploits sparsity is Dictionary Learning (DL), in which the coefficient matrix is constrained to be sparse. In DL, sparsity is in principle imposed in two main ways: Either column of \mathbf{S} is separately constrained to be sparse, e.g. $\|\mathbf{s}_i\|_0 \leq \gamma_i$, where γ_i is the maximum number of the non-zeros values of the i th column of \mathbf{S} , or the full coefficient matrix is directly constrained to have γ non-zeros [16], [21], [25]. In the fMRI context, the column-wise sparsity constraint corresponds to imposing sparsity per voxel; that is, the number of active sources that each source can have is constrained to be sparse. But this piece of information is voxel-dependent and is hard to accommodate in general. On the other hand, enforcing sparsity in the full coefficient matrix is easier to manage, but it still restrictive; since available spatial map-level information can not be implemented in a source by source basis.

In this paper, to the best of our knowledge, it is the first time that the DL framework is extended in order to allow sparsity promotion among rows (or sets of rows) of the coefficient matrix. Indeed, this development perfectly fits in the

fMRI analysis, but it also can be extended to other fields where DL is adopted as Blind Source Separation (BSS), e.g. in the hyperspectral imaging context. Thus, back to the problem in Eq. (2), the ℓ_0 -norm constitutes the best candidate to impose sparsity constraints. Imposing sparsity per rows, one admissible set of coefficient matrices can be defined as:

$$\mathfrak{L}_0 = \{ \mathbf{S} \in \mathbb{R}^{K \times N} \mid \| \mathbf{s}^i \|_0 \leq \phi_i \quad \forall i = 1, 2, \dots, K \}, \quad (5)$$

where ϕ_i is a user-defined parameter, which denotes the maximum number of non-zeros values of the i th row of the matrix \mathbf{S} . As it will be later discussed, such constraint bears physical meaning that renders ϕ_i values easily tunable in practice.

The implementation of the ℓ_0 -norm often results in an NP-hard task. For this reason, the ℓ_1 -norm has been widely adopted as a *convex* relaxation, since have been already established that under certain conditions both minimization problems are equivalent.

In this way, by replacing the ℓ_0 -norm with the ℓ_1 -norm the previous constrained set becomes:

$$\mathfrak{L}_1 = \{ \mathbf{S} \in \mathbb{R}^{K \times N} \mid \| \mathbf{s}^i \|_1 \leq \lambda_i \quad \forall i = 1, 2, \dots, K \}, \quad (6)$$

where λ_i are *new* extra user-defined parameters to implicitly control the sparsity of the rows of the coefficient matrix. In contrast to the parameters ϕ_i , the new parameters, λ_i , are unconnected to the level of sparsity, rendering them hard to tune in practice, unless cross validation is employed.

Consequently, in order to face all these critical issues introduced by this convex relaxation, the weighted ℓ_1 -norm is proposed as an alternative sparsifying constraint.

2.2. The weighted ℓ_1 -norm

Given an arbitrary vector $\mathbf{x} \in \mathbb{R}^N$, the weighted ℓ_1 -norm is defined as:

$$\| \mathbf{x} \|_{1, \mathbf{w}} = \sum_{i=1}^N w_i |x_i|, \quad (7)$$

where $\mathbf{w} > 0$ is the vector of weights, associated with. According to [26], [27], the values of the weights are set equal to:

$$w_i = \frac{1}{|x_i| + \varepsilon} \quad \forall i = 1, 2, \dots, N, \quad (8)$$

where $\varepsilon \in \mathbb{R}^+$ is a real positive number, which is introduced in order to avoid division by zero, providing enhanced numerical stability [2]. Under the above definition of weights, the weighted ℓ_1 -norm constitutes a good approximation of the ℓ_0 -norm [27]. Accordingly, a newly defined constrained set for the coefficient matrix is the following:

$$\mathfrak{L}_w = \{ \mathbf{S} \in \mathbb{R}^{K \times N} \mid \| \mathbf{s}^i \|_{1, \mathbf{w}^i} \leq \phi_i \quad \forall i = 1, 2, \dots, K \}, \quad (9)$$

where ϕ_i is *exactly the same* user-defined parameter as it was introduced in Eq. (5) and \mathbf{w}^i is the vector of weights defined as in Eq. (8). Here it is the key point: ϕ_i stands for the the maximum number of non-zero values, exactly in the same way as the ℓ_0 -norm.

However, this is not the only admissible constrained set, the weighted ℓ_1 -norm constrain can be alternatively imposed over the full the coefficient matrix as well:

$$\mathcal{L}_W = \left\{ \mathbf{S} \in \mathbb{R}^{K \times N} \mid \|\mathbf{S}\|_{1, \mathbf{W}} \leq \Phi \right\}, \quad (10)$$

where Φ is the maximum number of non-zero elements of the coefficient matrix \mathbf{S} and $\mathbf{W} \in \mathbb{R}^{K \times N}$ is the matrix of the associated weights defined as $\mathbf{W} = (w_{ij})_{ij}$ with $w_{ij} = \frac{1}{|s_{ij}| + \varepsilon}$. The notation $\|\cdot\|_{1, \mathbf{W}}$ stands for a generalization of the weighted ℓ_1 -nor for matrices, which is compactly written as:

$$\|\mathbf{S}\|_{1, \mathbf{W}} = \text{tr} [|\mathbf{S}| \mathbf{W}^T], \quad (11)$$

where $|\mathbf{S}|$ returns the absolute value of each element of \mathbf{S} .

At this point, observe that knowing the values ϕ_i , it is possible to set the sparsity level of \mathcal{L}_W as $\Phi = \sum_{i=1}^K \phi_i$ forcing both constrained sets to lead to the seam overall sparsity of \mathbf{S} . However, in the case of \mathcal{L}_w , the parameters ϕ_i impose a specific structure, which restricts the set of admissible coefficient matrices. In fact, \mathcal{L}_w is a subset of \mathcal{L}_W . This has relevant consequences to be analyzed in detail in Section 4.

General Case

From a more general perspective, we can see the sets \mathcal{L}_W and \mathcal{L}_w as two particular cases of a more general constrained set. In order to exploit this, let us first to define as \mathcal{B} a set containing a subset of M elements of the set $\{1, 2, \dots, K\}$ and as $\mathbf{S}_{\mathcal{B}}$ a row submatrix of \mathbf{S} comprising the rows of \mathbf{S} listed in the set \mathcal{B} . Then, a generalized constraint set is defined as:

$$\mathcal{L}_{\mathcal{B}} = \left\{ \mathbf{S} \in \mathbb{R}^{K \times N} \mid \|\mathbf{S}_{\mathcal{B}_i}\|_{1, \mathbf{W}_{\mathcal{B}_i}} \leq \phi_i, \forall i = 1, 2, \dots, B \right\}, \quad (12)$$

where ϕ_i , now, is the expected number of non-zero elements of the i^{th} submatrix $\mathbf{S}_{\mathcal{B}_i}$, $\mathbf{W}_{\mathcal{B}_i}$ is the associated submatrix of weights and B is the total number of submatrices considered.

Then, the set \mathcal{L}_w corresponds to the case of $\mathcal{B}_i = i$, where, $i = 1, 2, \dots, K$, whereas \mathcal{L}_W corresponds to the case where all the row indexes of the matrix are considered within the same set, i.e., $\mathcal{B}_i = \mathcal{B} = 1, 2, \dots, K$. Beyond these two particular cases defined above, this new set assembles a plethora of constrained sets just using different sets to index the matrix \mathbf{S} . Thus, we can study all these different cases under a single framework, using the general constrained set.

2.3. Supervised Dictionary Learning

As already discussed, a method called *Supervised Dictionary Learning* (SDL) [21] allows the incorporation of external information from the task-related time courses in the DL framework.

The starting point in the formulation of the SDL lies on splitting the dictionary in two parts:

$$\mathbf{D} = [\mathbf{\Delta}, \mathbf{D}_F] \in \mathbb{R}^{T \times K}, \quad (13)$$

where the first part, $\mathbf{\Delta} \in \mathbb{R}^{T \times M}$, is fixed and equal to the imposed task-related time courses. On the contrary, the second part, $\mathbf{D}_F \in \mathbb{R}^{T \times (K-M)}$, is left to vary and it is estimated via DL optimization arguments.

However, this approach still inherits the major drawbacks associated with GLM; the constrained dictionary atoms (columns of the matrix $\mathbf{\Delta}$) lead to improvement only if the imposed task-related time courses are sufficiently accurate. If the imposed task-related time courses are miss-modeled, their contributions can introduce detrimental effects, leading to wrong results.

2.4. Assisted Dictionary Learning

In this paper, an alternative approach is presented, which incorporates modified set of constraints that are associated with the task-related time courses. Specifically, the strong *equality* requirement from the previous approach is relaxed by a looser *similarity* distance-measuring norm constraint. Then, if part of the a priori information is inaccurate, the method is able to adjust the constrained atoms in an optimal way, since they are not enforced to be constant.

The starting point is again based on splitting the dictionary in two parts:

$$\mathbf{D} = [\mathbf{D}_C, \mathbf{D}_F] \in \mathbb{R}^{T \times K} \quad (14)$$

where, in contrast to the SDL approach, the part, $\mathbf{D}_C \in \mathbb{R}^{T \times M}$ is constrained to be *similar* to the imposed task-related time courses.

Then, the new *convex* set of dictionaries is defined as:

$$\mathfrak{D}_\delta = \left\{ \mathbf{D} \in \mathbb{R}^{T \times K} \mid \begin{array}{ll} \|\mathbf{d}_i - \boldsymbol{\delta}_i\|_2^2 \leq c_\delta & i = 1, \dots, M \\ \|\mathbf{d}_i\|_2^2 \leq c_d & i = M + 1, \dots, K \end{array} \right\} \quad (15)$$

where $\|\cdot\|_2$ denotes the Euclidean norm, \mathbf{d}_i is the i^{th} column of the dictionary \mathbf{D} and $\boldsymbol{\delta}_i$ is the i^{th} a priori selected task-related time course. The constant c_δ is a user-defined parameter, which controls the *degree of similarity* between the constrained atoms and the imposed time courses.

In practice, ill conditioned phenomena may occur associated to this kind of matrix factorization approaches [28]. Hence, in order to prevent degenerated solutions, the free atoms of the dictionary are constrained to have a bounded norm controlled by c_d , a user-defined parameter, which is usually set to 1 for simplicity.

3. Proposed Algorithm

In this Section, we present a new algorithm, called Assisted weighted Dictionary Learning (AwDL), to solve Eq. (2), incorporating the new proposed sets of constraints. Put succinctly, the new optimization task is cast as:

$$(\hat{\mathbf{D}}, \hat{\mathbf{S}}) = \underset{\mathbf{D}, \mathbf{S}}{\operatorname{argmin}} \|\mathbf{X} - \mathbf{D}\mathbf{S}\|_F^2 \quad \text{st.} \quad \begin{array}{l} \mathbf{D} \in \mathfrak{D}_\delta \\ \mathbf{S} \in \mathfrak{L}_B \end{array}, \quad (16)$$

where \mathfrak{D}_δ and \mathfrak{L}_B are the new constrained sets proposed before.

However, the simultaneous minimization with respect to \mathbf{D} and \mathbf{S} is a challenging one. In order to solve it, the *Block Majorized Minimization* (BMM) algorithm is adopted. This procedure is not new and it has been already used in several works, e.g. [29]. Essentially, the BMM algorithm simplifies the optimization task by adopting a two-step alternating minimization, under certain assumptions.

In particular, starting from an arbitrary set of estimates, $\mathbf{D}^{[0]}$ and $\mathbf{S}^{[0]}$, at the k^{th} iteration, the algorithm comprises the following steps:

$$\text{I. } \mathbf{S}^{[k+1]} = \min_{\mathbf{S}} \psi_S(\mathbf{S}, \mathbf{S}^{[k]}) \text{ s.t. } \mathbf{S} \in \mathfrak{L}_B, \quad (17)$$

$$\text{II. } \mathbf{D}^{[k+1]} = \min_{\mathbf{D}} \psi_D(\mathbf{D}, \mathbf{D}^{[k]}) \text{ s.t. } \mathbf{D} \in \mathfrak{D}_\delta, \quad (18)$$

where, according to the assumptions underlying any BMM algorithm, ψ_S is the surrogate function of the first step, given \mathbf{D} fixed to its current value $\mathbf{D}^{[k]}$ and ψ_D is the corresponding surrogate function of the second step, given \mathbf{S} fixed to its current value $\mathbf{S}^{[k+1]}$.

Hence, for each step, the main loss function is replaced by a surrogate function, which majorizes it and it is easier to be minimized compared to the original one. In general, the surrogate function is not unique but it has to satisfy certain specific conditions [29].

3.1. Step I: Coefficient Update

According to Eq. (17), the update step at the k^{th} iteration is formulated as:

$$\mathbf{S}^{[k+1]} = \min_{\mathbf{S}} \psi_S(\mathbf{S}, \mathbf{S}^{[k]}) \text{ s.t. } \mathbf{S} \in \mathfrak{L}_B.$$

Regarding the surrogate function ψ_S , an admissible candidate, which facilitates the optimization task in this case, can be obtained using a second order Taylor's expansion. e.g. see [29], i.e.:

$$\begin{aligned} \psi_S(\mathbf{S}, \mathbf{S}^{[k]}) &= \|\mathbf{X} - \mathbf{D}\mathbf{S}\|_F^2 - \left\| \mathbf{D}\mathbf{S} - \mathbf{D}\mathbf{S}^{[k]} \right\|_F^2 + \\ &+ c_S \left\| \mathbf{S} - \mathbf{S}^{[k]} \right\|_F^2, \end{aligned} \quad (19)$$

where $c_S \geq \|\mathbf{D}^T \mathbf{D}\|$ is a constant and $\|\cdot\|$ stands for the spectral norm.

Then, in order to solve the current task, the Lagrangian relaxation method is implemented. Therefore, introducing the Lagrange multipliers, the task becomes:

$$\min_{\mathbf{S}} \psi_S(\mathbf{S}, \mathbf{S}^{[k]}) + \mathcal{P}_\gamma(\mathbf{S}), \quad (20)$$

where \mathcal{P}_γ is a penalty term which depends on the weighted ℓ_1 -norm constraints and it is defined as:

$$\mathcal{P}_\gamma(\mathbf{S}) = \sum_{i=1}^B \gamma_i \left(\|\mathbf{S}_{\mathcal{B}_i}\|_{1, \mathbf{W}_{\mathcal{B}_i}} - \phi_i \right), \quad (21)$$

where the introduced parameters $\gamma_i \geq 0$, for $i = 1, 2, \dots, B$ are the Lagrange multipliers and B is the number of different submatrices considered.

From the theory of optimization, at the optimal point, the Lagrange multipliers have to satisfy the corresponding KKT conditions, i.e.,

$$\gamma_i \left(\|\mathbf{S}_{\mathcal{B}_i}\|_{1, \mathbf{w}_{\mathcal{B}_i}} - \phi_i \right) = 0, \quad (22)$$

with $i = 1, 2, \dots, B$.

Observe that the optimization task in Eq. (20) involves a *convex* loss function. Then, a global minimum exists at the k^{th} iteration. This is a nice feature and at the same time is a requirement as part of the sufficient conditions that guarantee the convergence of the BMM algorithm [30].

Although the loss function is convex, it is not differentiable. Nevertheless, the minimum can be obtained as a point with zero subgradient. That is, a minimizer of the function exists if and only if the zero (matrix) belongs to the subdifferential set given by:

$$\mathbf{0} \in \partial \left(\psi_S(\mathbf{S}, \mathbf{S}^{[k]}) + \mathcal{P}_\gamma(\mathbf{S}) \right). \quad (23)$$

In this case, the first terms is fully differentiable, then, the subdifferential becomes a singleton given by the standard derivative:

$$\begin{aligned} \partial \left(\psi_S(\mathbf{S}, \mathbf{S}^{[k]}) \right) &= \left\{ \nabla \psi_S(\mathbf{S}, \mathbf{S}^{[k]}) \right\} = \\ &= \left\{ -2\mathbf{D}^T \mathbf{X} + 2c_S \mathbf{S} - 2c_S \mathbf{S}^{[k]} - 2\mathbf{D}\mathbf{D}^T \mathbf{S}^{[k]} \right\}, \end{aligned}$$

that is,

$$\partial \left(\psi_S(\mathbf{S}, \mathbf{S}^{[k]}) \right) = \{ 2c_S(\mathbf{S} - \mathbf{A}) \}, \quad (24)$$

where \mathbf{A} is a new introduced matrix defined as:

$$\mathbf{A} \triangleq \frac{1}{c_S} \left[\mathbf{D}^T \mathbf{X} + (c_S \mathbf{I}_K + \mathbf{D}^T \mathbf{D}) \mathbf{S}^{[k]} \right]. \quad (25)$$

With respect to the second term, it is not differentiable, but, its corresponding subdifferential set is given by:

$$\partial \mathcal{P}_\gamma(s_{ij}) = \begin{cases} \gamma_i w_{ij} \text{sign}(s_{ij}) & \text{if } s_{ij} \neq 0 \\ \gamma_i w_{ij} g_{ij} \text{ with } g_{ij} \in [-1, 1] & \text{if } s_{ij} = 0 \end{cases}. \quad (26)$$

However, this set depends on the specific selection of the imposed Lagrange multipliers γ_i , which are determined via the associated KKT conditions, i.e.:

$$\gamma_i (\|\mathbf{S}_{\mathcal{B}_i}\|_{1, \mathbf{w}_{\mathcal{B}_i}} - \phi_i) = 0 \quad \forall i = 1, 2, \dots, B.$$

Therefore, the final problem is to find the matrix \mathbf{S} from the subdifferential set which simultaneously satisfies

$$2c_S(\mathbf{S} - \mathbf{A}) + \partial \mathcal{P}_\gamma(\mathbf{S}) = \mathbf{0}$$

and its corresponding KKT conditions, where $\partial\mathcal{P}_\gamma$ is given by Eq. (26).

Thus, following standard arguments and after some algebraic manipulations, it can be shown that the solution is given by:

$$\mathbf{S}_{\mathcal{B}_i} = \begin{cases} \mathbf{A}_{\mathcal{B}_i} & \text{if } \|\mathbf{A}_{\mathcal{B}_i}\|_{1, \mathbf{W}_{\mathcal{B}_i}} \leq \phi_i \\ \mathcal{P}_{B_{\ell_1}[\mathbf{W}_{\mathcal{B}_i}, \phi_i]}(\mathbf{A}_{\mathcal{B}_i}) & \text{if } \|\mathbf{A}_{\mathcal{B}_i}\|_{1, \mathbf{W}_{\mathcal{B}_i}} > \phi_i \end{cases}, \quad (27)$$

with $i = 1, 2, \dots, B$, where $\mathbf{S}_{\mathcal{B}_i}$ and $\mathbf{A}_{\mathcal{B}_i}$ are the submatrix of the coefficient matrix and the matrix \mathbf{A} indexed by the i^{th} tuple, respectively, matrix $\mathbf{W}_{\mathcal{B}_i}$ is the corresponding sub-matrix of weights, and $\mathcal{P}_{B_{\ell_1}[\mathbf{W}_{\mathcal{B}_i}, \phi_i]}$ is the projection operator over the weighted ℓ_1 -norm ball, $B_{\ell_1}[\mathbf{W}_{\mathcal{B}_i}, \phi_i]$ of weights $\mathbf{W}_{\mathcal{B}_i}$ of radius ϕ_i .

For the projection over the weighted ℓ_1 -norm ball, many available algorithms can be implemented, e.g., [27]. Nevertheless, the majority of those algorithms are designed for vectors. Then, in order to apply the solution in Eq. (27), each submatrix must be properly vectorized prior to their application. This operation is an isomorphism, which does not disrupt the projection.

With respect to the associated Lagrange multipliers, γ_i , the values are given by:

$$\gamma_i = \max \left\{ 0, \frac{2c_S(\|\mathbf{A}_{\mathcal{B}_i}\|_{1, \mathbf{W}_{\mathcal{B}_i}} - \phi_i)}{\|\mathbf{W}_{\mathcal{B}_i}\|_F^2} \right\}. \quad (28)$$

Finally, the coefficient update can be compactly written by introducing a new operator:

$$\mathbf{S}^{[k+1]} = \mathcal{Q}_B(\mathbf{A}), \quad (29)$$

where $\mathcal{Q}_B(\mathbf{A}) : \mathbf{A}_{\mathcal{B}_i} \rightarrow \mathbf{S}_{\mathcal{B}_i}^{[k+1]}$ with $i = 1, 2, \dots, B$ controls the update for each sub-matrix and it is defined via the solution provided in Eq. (27), that is,

$$\mathbf{S}_{\mathcal{B}_i}^{[k+1]} = \begin{cases} \mathbf{A}_{\mathcal{B}_i} & \text{if } \|\mathbf{A}_{\mathcal{B}_i}\|_{1, \mathbf{W}_{\mathcal{B}_i}} \leq \phi_i \\ \mathcal{P}_{B_{\ell_1}[\mathbf{W}_{\mathcal{B}_i}, \phi_i]}(\mathbf{A}_{\mathcal{B}_i}) & \text{if } \|\mathbf{A}_{\mathcal{B}_i}\|_{1, \mathbf{W}_{\mathcal{B}_i}} > \phi_i \end{cases},$$

where the parameters are the same as they were described above.

Iterative Weight Estimates

Theoretically, the best possible value for the weights corresponds to the optimal solution of the main optimization task. Of course, this is impossible in practice, since the solution is unknown. However, one can use the currently available estimates according to Eq. (8). Indeed, this iterative update tends to obtain successively better estimates of the weights, and it is smoothly integrated within the optimization process [26], [27].

3.2. Step II: Dictionary Update

In the second step of the alternating minimization, i.e. Eq. (18), the optimization task at the k^{th} step is:

$$\mathbf{D}^{[k+1]} = \min_{\mathbf{D}} \psi_D(\mathbf{D}, \mathbf{D}^{[k]}) \quad \text{s.t.} \quad \mathbf{D} \in \mathfrak{D}_\delta.$$

With respect to the surrogate function, ψ_D , an admissible choice can be obtained from a second order Taylor's expansion [29] around \mathbf{D}^k , that is,

$$\begin{aligned} \psi_D(\mathbf{D}, \mathbf{D}^{[k]}) &= \|\mathbf{X} - \mathbf{D}\mathbf{S}\|_F^2 - \|\mathbf{D}\mathbf{S} - \mathbf{D}^{[k]}\mathbf{S}\|_F^2 + \\ &+ c_D \|\mathbf{D} - \mathbf{D}^{[k]}\|_F^2, \end{aligned} \quad (30)$$

where $c_D \geq \|\mathbf{S}\mathbf{S}^T\|$ and $\|\cdot\|$ stands for the spectral norm.

In order to solve the current task, the BMM algorithm does not impose any restrictions. For simplicity, a Lagrangian relaxation is again implemented. Thus, introducing a new penalty term, the original task can be rewritten as:

$$\min_{\mathbf{D}} \psi_D(\mathbf{D}, \mathbf{D}^{[k]}) + \mathcal{P}_\gamma(\mathbf{D}), \quad (31)$$

where \mathcal{P}_γ is defined according to the constraints over the dictionary:

$$\begin{aligned} \mathcal{P}_\gamma(\mathbf{D}) &= \sum_{i=1}^M \gamma_i [(\mathbf{d}_i - \boldsymbol{\delta}_i)^T (\mathbf{d}_i - \boldsymbol{\delta}_i) - c_\delta] + \\ &+ \sum_{i=M+1}^K \gamma_i (\mathbf{d}_i^T \mathbf{d}_i - c_d), \end{aligned} \quad (32)$$

where γ_i , $i = 1, 2, \dots, K$ are the respective K Lagrange multipliers.

Note that $\mathcal{P}_\gamma(\mathbf{D})$ is formed by two different terms; the first one refers to the first M columns of the dictionary and it "deals" with the similarity constraint. The second relates to the remaining $(K - M)$ columns that impose a penalization over the respective norms.

The associated KKT conditions are given by:

$$\gamma_i \left(\|\mathbf{d}_i - \boldsymbol{\delta}_i\|^2 - c_\delta \right) = 0 \quad i = 1, 2, \dots, M, \quad (33)$$

$$\gamma_i \left(\|\mathbf{d}_i\|^2 - c_d \right) = 0 \quad i = M + 1, \dots, K. \quad (34)$$

For simplicity, the term in Eq. (32) can be rewritten in a more compact form by introducing the following matrix notation: Define the mask matrix $\mathbf{M} \in \mathbb{R}^{M \times K}$, which is a rectangular matrix ($M < K$) with zero elements everywhere except the elements along its principal diagonal, which are equal to one, i.e.,

$$\mathbf{M} \triangleq (m_{ij})_{ij} \longrightarrow \begin{cases} m_{ij} = 0 & \text{if } i \neq j \\ m_{ij} = 1 & \text{if } i = j \end{cases}. \quad (35)$$

Using this mask matrix and the properties of the trace, we can compactly write:

$$\mathcal{P}_\Gamma(\mathbf{D}) = \text{tr} \left[\Gamma \left((\mathbf{D} - \mathbf{\Delta M})^T (\mathbf{D} - \mathbf{\Delta M}) - \mathbf{C} \right) \right],$$

where $\mathbf{\Gamma}$ is a diagonal matrix $\mathbf{\Gamma} = \text{diag}\{\gamma_1, \gamma_2, \dots, \gamma_K\}$ and \mathbf{C} is another diagonal matrix given by $\mathbf{C} = \text{diag}\{c_d \mathbf{1}_M, c_d \mathbf{1}_{K-M}\}$.

Eventually, the minimization task for this step is compactly written as:

$$\mathbf{D}^{[k+1]} = \min_{\mathbf{D}} \psi_D(\mathbf{D}, \mathbf{D}^{[k]}) + \mathcal{P}_{\mathbf{\Gamma}}(\mathbf{D}).$$

The current loss function is *convex*, for fixed \mathbf{S} to its current estimate $\mathbf{S} = \mathbf{S}^{[k+1]}$, and a global minimum exists at the k^{th} iteration. Besides, as it was described before, the uniqueness is also a sufficient condition to guarantee the convergence of the BMM algorithm [30].

In this case, the loss function is fully differentiable and the minimum is found as the point with the zero gradient, i.e.:

$$\nabla_{\mathbf{D}} \left(\psi_D(\mathbf{D}, \mathbf{D}^{[k]}) + \mathcal{P}_{\mathbf{\Gamma}}(\mathbf{D}) \right) = 0. \quad (36)$$

The derivative of the first term is given by:

$$\nabla_{\mathbf{D}} \psi_D = -2\mathbf{X}\mathbf{S}^T + 2\mathbf{D}^{[k]}\mathbf{S}\mathbf{S}^T + 2c_D\mathbf{D} - 2c_D\mathbf{D}^{[k]},$$

and the derivative of the second term is given by:

$$\nabla_{\mathbf{D}} \mathcal{P}_{\mathbf{\Gamma}}(\mathbf{D}) = 2\mathbf{D}\mathbf{\Gamma} - 2\mathbf{\Delta}\mathbf{M}\mathbf{\Gamma},$$

Now, solving with respect to \mathbf{D} results to:

$$\mathbf{D} = \left[\mathbf{B} + \frac{1}{c_D} \mathbf{\Delta}\mathbf{M}\mathbf{\Gamma} \right] \left(\frac{1}{c_D} \mathbf{\Gamma} + \mathbf{I}_K \right)^{-1}, \quad (37)$$

where \mathbf{B} is a matrix defined as:

$$\mathbf{B} \triangleq \frac{1}{c_D} \left[\mathbf{X}\mathbf{S}^T + \mathbf{D}^{[k]} (c_D \mathbf{I}_K - \mathbf{S}\mathbf{S}^T) \right],$$

and the Lagrange multipliers in $\mathbf{\Gamma}$ are obtained so that to satisfy the corresponding KKT conditions.

A careful observation of the previous set of equations reveals that the solution is separable; thus, one can equivalently write K equations, one for each specific column of \mathbf{D} , that is:

$$\mathbf{d}_i = \left[\mathbf{b}_i + \frac{1}{c_D} m_i \boldsymbol{\delta}_i \gamma_i \right] \left(\frac{\gamma_i}{c_D} + 1 \right)^{-1},$$

with $i = 1, 2, \dots, K$ and m_i is defined so that $m_i = 1$ if $i \leq M$ and $m_i = 0$ if $i > M$. Defining $\mu_i = \frac{c_D}{c_D + \gamma_i}$, the previous expression can be easily written as:

$$\mathbf{d}_i = \mu_i \mathbf{b}_i + m_i (1 - \mu_i) \boldsymbol{\delta}_i. \quad (38)$$

Note that according to the values of m_i , these equations can be divided in two different groups:

$$\mathbf{d}_i = \mu_i \mathbf{b}_i + (1 - \mu_i) \boldsymbol{\delta}_i \quad i = 1, 2, \dots, M, \quad (39)$$

$$\mathbf{d}_i = \mu_i \mathbf{b}_i \quad i = M + 1, \dots, K, \quad (40)$$

that is, one for each constrained part of the dictionary.

Similarity Constraint

Eq. (39) stands for the similarity constraints, whose associated KKT conditions are given by $\gamma_i \left(\|\mathbf{d}_i - \boldsymbol{\delta}_i\|^2 - c_\delta \right) = 0$. Hence, only two solutions are admissible: $\gamma_i = 0$ or $\|\mathbf{d}_i - \boldsymbol{\delta}_i\|^2 = c_\delta$.

Then, according to the dictionary constraint, it can be shown, that

$$\text{if } \|\mathbf{b}_i - \boldsymbol{\delta}_i\|^2 \leq c_\delta \Leftrightarrow \gamma_i = 0,$$

is a correct solution, and the update is easily written as $\mathbf{d}_i^{[k+1]} = \mathbf{d}_i = \mathbf{b}_i$.

On the other hand, if $\|\mathbf{b}_i - \boldsymbol{\delta}_i\|^2 > c_\delta$, the selection of $\gamma_i = 0$ is not admissible. However, if $\gamma_i \neq 0$, according to the KKT conditions, it necessarily leads to:

$$\|\mathbf{d}_i - \boldsymbol{\delta}_i\|^2 = c_\delta,$$

where by definition,

$$\|\mathbf{d}_i - \boldsymbol{\delta}_i\|^2 = \mu_i^2 \|\mathbf{b}_i - \boldsymbol{\delta}_i\|^2 = c_\delta.$$

Thus,

$$\mu_i = \frac{c_\delta^{1/2}}{\|\mathbf{b}_i - \boldsymbol{\delta}_i\|} \Rightarrow \gamma_i = c_D \left(\frac{1}{\mu_i} - 1 \right).$$

Finally, the dictionary part for the similarity constraint can be written as:

$$\mathbf{d}_i^{[k+1]} = \begin{cases} \mathbf{b}_i & \text{if } \|\mathbf{b}_i - \boldsymbol{\delta}_i\|^2 \leq c_\delta \\ \frac{c_\delta^{1/2} (\mathbf{b}_i - \boldsymbol{\delta}_i)}{\|\mathbf{b}_i - \boldsymbol{\delta}_i\|} + \boldsymbol{\delta}_i & \text{if } \|\mathbf{b}_i - \boldsymbol{\delta}_i\|^2 > c_\delta \end{cases}, \quad (41)$$

with $i = 1, 2, \dots, M$.

Normalization Constraint

With respect to the normalization constrain Eq. (40), the KKT conditions are given by $\gamma_i \left(\|\mathbf{d}_i\|^2 - c_d \right) = 0$ which has two admissible solutions: $\gamma_i = 0$ or $\|\mathbf{d}_i\|^2 = c_d$, for $i = M + 1, M + 2, \dots, K$.

Again, it can be shown that,

$$\text{if } \|\mathbf{b}_i\|^2 \leq c_d \Leftrightarrow \gamma_i = 0$$

is a solution and the update step can be easily written as $\mathbf{d}_i^{[k+1]} = \mathbf{d}_i = \mathbf{b}_i$.

However, if $\|\mathbf{b}_i\|^2 > c_d$, the solution $\gamma_i = 0$ is not admissible anymore; if, $\gamma_i \neq 0$, then, the KKT conditions impose that,

$$\|\mathbf{d}_i\|^2 = c_d.$$

By definition,

$$\|\mathbf{d}_i\|^2 = \mu_i^2 \|\mathbf{b}_i\|^2 = c_d,$$

that is,

$$\mu_i = \frac{c_d^{1/2}}{\|\mathbf{b}_i\|} \Rightarrow \gamma_i = c_D \left(\frac{1}{\mu_i} - 1 \right).$$

Eventually, for the normalization constraint, the update step it can be written as:

$$\mathbf{d}_i^{[k+1]} = \begin{cases} \mathbf{b}_i & \text{if } \|\mathbf{b}_i\|^2 \leq c_d \\ \frac{c_d^{1/2}}{\|\mathbf{b}_i\|} \mathbf{b}_i & \text{if } \|\mathbf{b}_i\|^2 > c_d \end{cases}, \quad (42)$$

with $i = M + 1, M + 2, \dots, K$.

Thus, the dictionary update can be compactly performed introducing a new operator:

$$\mathbf{D}^{[k+1]} = \mathcal{U}(\mathbf{B}), \quad (43)$$

where $\mathcal{U}(\mathbf{B}) : \mathbf{b}_i \rightarrow \mathbf{d}_i$ with $i = 1, 2, \dots, K$, it controls the two possible alternatives and it is defined as:

$$\mathbf{d}_i = \begin{cases} i \leq M & \begin{cases} \mathbf{b}_i & \text{if } \|\mathbf{b}_i - \boldsymbol{\delta}_i\|^2 \leq c_\delta \\ \frac{c_\delta^{1/2}(\mathbf{b}_i - \boldsymbol{\delta}_i)}{\|\mathbf{b}_i - \boldsymbol{\delta}_i\|} + \boldsymbol{\delta}_i & \text{otherwise} \end{cases} \\ i > M & \begin{cases} \mathbf{b}_i & \text{if } \|\mathbf{b}_i\|^2 \leq c_d \\ \frac{c_d^{1/2}}{\|\mathbf{b}_i\|} \mathbf{b}_i & \text{otherwise} \end{cases} \end{cases}. \quad (44)$$

Pseudo-code

Put succinctly, the new algorithm for the proposed optimization task comprises in the following pseudo-code depicted below:

Proposed Algorithm

```

1  Initialization:  $\mathbf{S}^{[0]}, \mathbf{D}^{[0]}, \varepsilon > 0$ 
2   $k = 0$ 
3  repeat
4
5      Step I - Coefficient Update
6      Init:  $\mathbf{D} = \mathbf{D}^{[k]}, c_S \geq \|\mathbf{D}^T \mathbf{D}\|$ 
7       $\mathbf{A} = \frac{1}{c_S} [\mathbf{D}^T \mathbf{X} + (c_S \mathbf{I}_K - \mathbf{D}^T \mathbf{D}) \mathbf{S}^{[k]}]$ 
8       $\mathbf{W} \rightarrow w_{ij} = \frac{1}{|a_{ij}| + \varepsilon}$ 
8       $\mathbf{S}^{[k+1]} = \mathcal{Q}_B(\mathbf{A})$ 
9
10     Step II - Dictionary Update
11     Init:  $\mathbf{S} = \mathbf{S}^{[k+1]}, c_D \geq \|\mathbf{S} \mathbf{S}^T\|$ 
12      $\mathbf{B} = \frac{1}{c_D} [\mathbf{X} \mathbf{S}^T + \mathbf{D}^{[k]} (c_D \mathbf{I}_K - \mathbf{S} \mathbf{S}^T)]$ 
13      $\mathbf{D}^{[k+1]} = \mathcal{U}(\mathbf{B})$ 
14
15      $k = k + 1$ 
16
17 until some stopping criterion is satisfied
18 output:  $\mathbf{D}^{[k]}, \mathbf{S}^{[k]}$ 

```

3.3. Initialization

In general, DL algorithms are designed for solving non-convex problems, which are characterized by containing a huge number of potential local minima. Then, if a bad initialization estimates is adopted, any algorithm will likely converge to an undesirable solution. In fact, this is a common problem for all the matrix factorization-based techniques. For this reason, each specific algorithm considers the initialization that better suits its specific task.

Accordingly, different initialization procedures have been analyzed, being ICA the approach that exhibited the best performance. On despite of the aforementioned issues respect to ICA, the solution of ICA can constitute a good initialization procedure for DL algorithms [31].

Furthermore, using the solution of ICA as initialization of the proposed algorithms turns out a beautiful synergy: the algorithm starts from the solution of ICA and the DL scheme breaks the independence hypothesis limitations enhancing the total performance.

In this paper, we implement an ICA algorithm called JADE [32], which identifies independent components computing fourth-order cumulants. Afterwards we project the solution of JADE over the constrained set of matrices –using the defined weighted ℓ_1 -norm projector– to fits the solution of JADE in the imposed constrained set. Then, the results in used as initialization estimate of the coefficient matrix.

Of course, other advanced procedures or novel ICA algorithms can be applied. For example, alternative ICA method that simultaneously provides independent-

sparse decomposition [33] constitutes an interesting alternative or more recently in [34].

4. Performance evaluation

This section studies the performance of the newly proposed algorithm based on a synthetic but realistic data set.

4.1. Generation of a Realistic synthetic Data Set

In this paper, we present a new realistic synthetic data set using SimTB,¹ which enables a flexible composition of synthetic fMRI-like data sets and has been widely used in a number of fMRI studies, e.g., [36], [37], [38].

SimTB implements a simple spatiotemporal separable model, characterized by two features: a) the spatial maps are smooth (Gaussian-shaped) and b) the sources are barely overlapped; the overlap only affects small areas with low relative intensity. Both features are non-realistic, because real brain activity often exhibit non-linear effects, leading to the saturation of the brain response, and the overlap often affect extensive areas with high relative intensity.

For this reason, we modified the default sources of SimTB: first, instead of Gaussian shapes, which show activation at just one specific voxel, we rather prefer to have more than one neighbor voxel activated with the same relative energy. In order to do that, we started from the Gaussian shapes from SimTB, then, we reduce the highest activated voxels to have the same relative value. Finally, we rearranged in the space some of the sources to increase their overlap.

After these modifications, the final data set comprises 16 brain-like sources (see Fig. (1)); each source is formed by a single slice of size 100×100 voxels and a time course, which comprises 300 time instances with a difference of two second between consecutive acquisition times (TR=2).

Beyond the sources directly related to the brain activity, true fMRI data contain sources that are either scanner-induced or related to biological processes such as heart-beating, breathing, etc. All these phenomena are collectively referred as *artifacts*, and some of them exhibit large intensity compared with the brain-induced sources of interest. Accordingly, we included five extra sources from the data set in [18]. Precisely, the sources 3, 4, 5, 7 and 8 that represent fMRI-like artifacts (see Fig. (2)).

Finally, Table 1 summarizes the main features of the generated data set. Observe that the majority of the brain-like sources are sparse (like the natural brain activity behavior), where the artifacts are mostly dense.

Apart from brain-like sources and artifacts, fMRI data are corrupted by Rician noise [39]. In the next section, we will add Rician noise as an external component, with the aim to study the different considered algorithms under different scenarios and levels of noise [40].

¹SimTB is an open MATLAB toolbox for the creation of brain-like fMRI datasets. It can be downloaded from (<http://mialab.mrn.org/software>)

Brain-like Sources

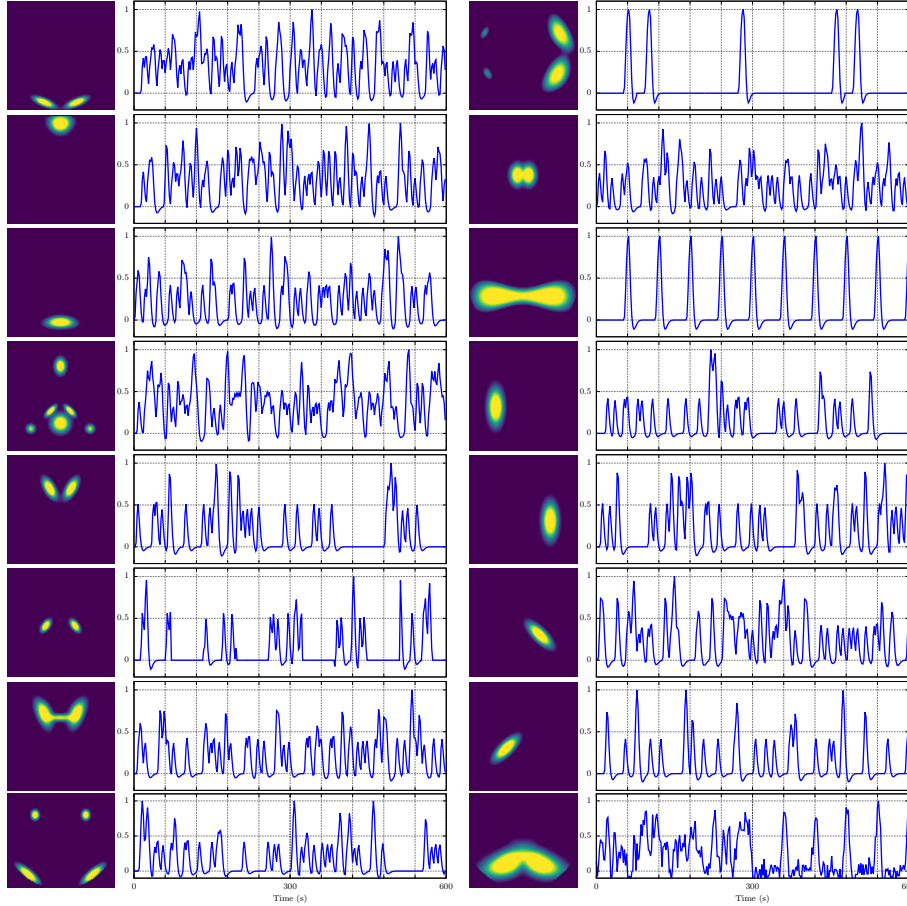


Figure 1: Spatial maps and their corresponding time courses of all the brain-like sources proposed for this synthetic data set.

Artifacts

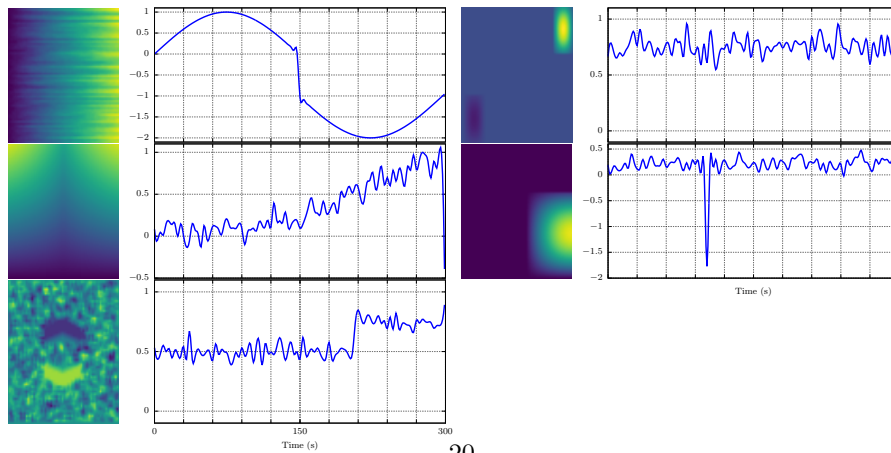


Figure 2: Artifacts from the data set [35]. The first column depicts the spatial maps and their corresponding time courses for the sources 3, 4 and 5 while the second column shows the sources 7 and 8.

Brain-like Sources		
Source	SimTB Correspondence	lvl. Sparsity
#	<i>Anatomical correspondence</i> [36]	
1	Bilateral Visual - more posterior	95.28 %
2	Medial Frontal	95.33 %
3	Precuneus	95.53 %
4	Default Mode Network	88.25 %
5	Subcortical nuclei	93.30 %
6	Subcortical nuclei - putamen	97.07 %
7	White matter tracts (anterior)	88.07 %
8	Dorsal Attention Network	91.82 %
9	Frontoparietal (Right dominance)	85.51 %
10	Subcortical nuclei - thalamus	92.67 %
11	SensoriMotor	77.38 %
12	Right Auditory	91.60 %
13	Left Auditory	91.53 %
14	Right Hippocampus	94.51 %
15	Left Hippocampus	94.57 %
16	White matter tracts (posterior)	71.95 %

Artifacts		
#	<i>Features according to</i> [35]	lvl. Sparsity
17	sub-Gaussian	1.00 %
18	Gaussian	1.00 %
19	super-Gaussian	1.99 %
20	sub-Gaussian	86.14 %
21	super-Gaussian	71.84 %

Mean values of the Levels of Sparsity	
Whole data set	76.49 %
Brain-like sources	90.27 %
Artifacts	32.39 %

Table 1: Summary of the main features of the proposed synthetic data set, including their corresponding level of sparsity. Observe that although the mean level of sparsity of the data set is 76.5%, the brain-like sources are clearly dominated by high level of sparsity, whereas the artifacts are mainly dense (see Fig. (1) and Fig. (2)).

4.2. Performance Study

In this section we analyze and compare the main features of the proposed method with other standard DL methods, using the new proposed synthetic data set. Thus, we divide this study in two different experiments, which will be focused in the two main novel constraints.

Experiment 1 - Analysis of the weighted ℓ_1 -norm

The first experiment aim to analyze the behavior of the weighted ℓ_1 -norm. In particular, we compare the performance of three different DL methods: a) an on-lined DL sparse coding algorithm from SPAMS package [41], b) a standard DL algorithm based on the Majorization Minimization method [25], and c) the new proposed DL algorithm.

For this case, we study the behavior of the different methods using the proposed synthetic data set for different noise levels. Although we have conducted several tests, implementing different number of sources, for simplicity, here we only report the case with the correct number of sources, which assembles the best scenario for all the studied methods.

Note that the first two proposed methods are base on the standard ℓ_1 -norm regularization (but with different implementations), this means that they require to tune an external parameter, λ , that controls the sparsity and depends on the number of sources, the data set and the level of noise.

In this experiment, since we know the correct solution, we optimize the respective regularization parameters in the noise-less case to obtain the best performance and we keep these values for the rest of noise levels. However, in real fMRI studies, cross validation arguments has no practical meaning; making the optimization of the regularization parameters a complicated time-consuming task.

Regarding to the proposed method, in this experiment we are focused on the study of the sparsity constraint. Thus, depending of the a priori sparsity information the user can define a plethora of sparsity constraints. In this case, we expose two limit cases:

- *Case (A)*: This case assembles the worst possible scenario: we do not consider any task-related time course and we only dispose a rough estimate of the expected mean value of the level of sparsity of the whole coefficient matrix. Then, the set of constraints for this case can be written as:

$$\begin{aligned} \mathfrak{L}_W &= \left\{ \mathbf{S} \in \mathbb{R}^{K \times N} \mid \|\mathbf{S}\|_{1, \mathbf{w}} \leq NL \right\}, \\ \mathfrak{D}_d &= \left\{ \mathbf{D} \in \mathbb{R}^{T \times K} \mid \|\mathbf{d}_i\|^2 \leq 1 \quad \forall i = 1, 2, \dots, K \right\}, \end{aligned}$$

where $N = 10000$ and $T = 300$ are the size of the synthetic data set. The level of sparsity L in this case is set equal to 70 %, which is a rough underestimate of the true mean level of sparsity 76.49 % (see Table 1).

- *Case (B)*: Again, we do not consider any task-related time course; the admissible set of dictionaries is equal to the case A, i.e. \mathfrak{D}_d . But, in this case we assume that we have some clues about the level of sparsity of the sources: for example, we expect that most of the brain-like sources are sparse, i.e. with a sparsity level over 80%; whereas artifacts are likely to be dense, i.e. with a sparsity level lower than 5%.

Thus, having these ideas in mind, we define a new constrained set of coefficient matrices as:

$$\mathfrak{L}_w = \left\{ \mathbf{S} \in \mathbb{R}^{K \times N} \mid \|\mathbf{s}^i\|_{1, \mathbf{w}^i} \leq Nl_i \quad \forall i = 1, 2, \dots, K \right\}$$

where l_i are the expected level of sparsity for each spatial map and K is the specific number of sources.

However, unlike standard ℓ_1 -norm approaches, we do not need to optimize the levels of sparsity. Instead, we use the natural information from the problem to impose an estimates of the different level of sparsity. Thus, the next Table shows the implemented levels of sparsity together with the exact values.

Correct	Estimated (1)
97.07	95
95.53	94
95.33	93
95.28	92
94.57	91
94.51	90
93.30	89
92.67	88
91.82	87
91.60	86
91.53	85
88.25	85
88.07	80
86.14	80
85.51	75
77.38	70
71.95	65
71.84	60
1.99	0
1.00	0
1.00	0

Table 2: Comparison between levels of sparsity

In the previous Table, we explicitly sorted the levels of sparsity in order to easily compare the values. But, in practice, ordering the levels of sparsity is optional; the user is free to use any arbitrary order. Observe also that three of the levels of sparsity were set to 0%, because we expected that at least three sources are going to be dense.

Finally, Fig. (3) shows the results of this experiment for the different studied methods. Every point represents the mean value for 100 different noise realizations with exactly the same parameters. The horizontal axis assembles different level of Rician noise. The vertical axis indicates the squared value of the mean Pearson correlation, R^2 , between the estimated decomposition and the correct one. That is:

$$R^2 = \left(\frac{1}{K} \sum_{i=1}^K \rho(\mathbf{F}_i, \hat{\mathbf{F}}_i) \right)^2, \quad (45)$$

where K is the total number of sources considered, \mathbf{F}_i is the i^{th} source of the decomposition, that is, $\mathbf{F}_i = \mathbf{d}_i \mathbf{s}^i$ where \mathbf{d}_i and \mathbf{s}^i are the i^{th} column of the dictionary, \mathbf{D} , and the i^{th} row of the coefficient matrix, \mathbf{S} , whereas $\hat{\mathbf{F}}_i$ is the corresponding true source from the synthetic data set.

With respect to $\rho(\mathbf{A}, \mathbf{B})$, with $\mathbf{A}, \mathbf{B} \in \mathbb{R}^{M \times N}$, it stands for the Pearson correlation, which is given by:

$$\rho(\mathbf{A}, \mathbf{B}) = \frac{1}{M + N - 1} \sum_{i,j=1}^{M,N} \left(\frac{a_{ij} - \mu_{\mathbf{A}}}{\sigma_{\mathbf{A}}} \right) \left(\frac{b_{ij} - \mu_{\mathbf{B}}}{\sigma_{\mathbf{B}}} \right) \quad (46)$$

where $\mu_{\mathbf{A}}$ and $\sigma_{\mathbf{A}}$ are the mean and the standard deviation of \mathbf{A} , respectively, and $\mu_{\mathbf{B}}$ and $\sigma_{\mathbf{B}}$ are the mean and the standard deviation of \mathbf{B} .

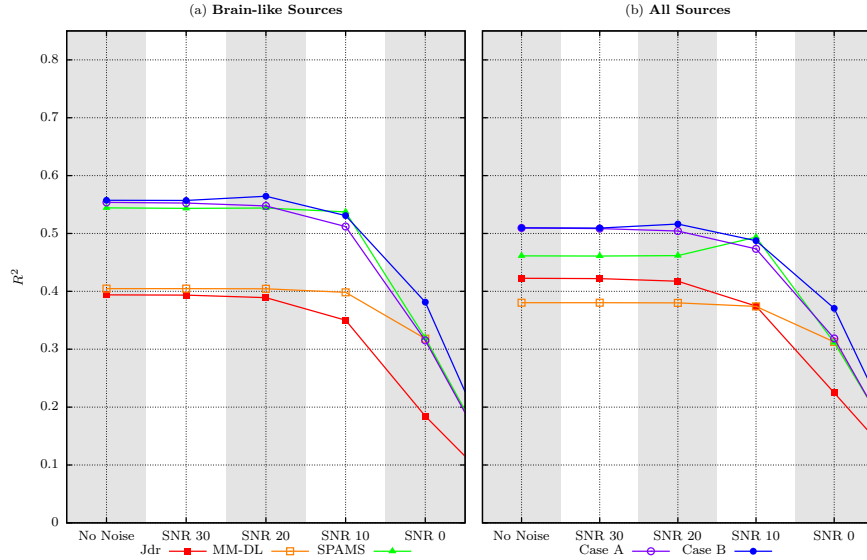


Figure 3: Result of the Experiment 1 – Mean performance of the different studied method for different level of Rician noise, for the correct number of sources $K = 21$.

Observe that all the considered DL algorithms perform better recovering brain-like sources (see Fig. (3.a)) rather than the artifacts (Fig. (3.b)). This is because most of the artifacts are dense, that is, they are more difficult to unmix via sparse assumptions. However, our method is less sensitive to this effects since it can explicitly target non-sparse sources. Regarding to the noise all the proposed methods have exhibited the same performance.

On the other hand, although we have encountered at the end similar performance between different implementations, the most important advantage introduced by the proposed constraint is that it does *not* require optimizing the regularization parameter; they were naturally selected from the problem information. Whereas, in MM-DL or in SPAM we optimize the regularization parameter through cross-validation to obtain near the same results.

Experiment 2 - Assisted weighted Dictionary Learning

The aim of this experiment is twofold: first, we study the performance of the proposed method when information related to the task-related time courses is imposed. As a benchmark, the Semi-blind Dictionary Learning (SDL) [21] method is used, since it is the only alternative DL-based approach which incorporates task-related time courses as external information. Second, we study the sensitivity of the aforementioned algorithms to the tuning of their free parameters, namely, the regularization parameter, λ , in the case of SDL and the per-row sparsity constraints of our proposed method.

We have chosen 3 different time courses from the synthetic dataset, in particular sources 1, 12 and 13, to be considered as task-related. The specific sources represent brain areas that are commonly targeted in practice and they exhibit overlap with their surrounding sources. Since one of the scopes of this experiment is to analyze the effect of mis-modeling of the imposed task-related time courses, we have to synthetically generate HRFs, which differ to a greater or lesser degree from the canonical HRF (shown in thick red line in Fig. (4)) that was used for the generation of the dataset. Then for each mis-modeled HRF the three aforementioned task-related time-courses can be computed and imposed in the studied methods.

Accordingly, we generated five different HRFs (shown with color lines in Fig. (4)) by feeding with randomly generated parameters the two-gamma distribution model [7], taking care, however, to keep the generated parameters within limits that resembles the expected variability and characteristics of actual HRFs. To confirm this, 100 HRFs were generated with the adopted randomized method (shown with gray lines in Fig. (4)) and visually compared to human brain HRFs that have been estimated in several studies, e.g. in [42].

With respect to the proposed algorithm, the user now can define both constraints using the task-related time courses as well as the level of sparsity per source. Thus, the constrained set of dictionaries can be written as following:

$$\mathfrak{D}_\delta = \left\{ \mathbf{D} \in \mathbb{R}^{T \times K} \mid \begin{array}{ll} \|\mathbf{d}_i - \delta_i\|^2 \leq c_\delta & i = 1, 2, 3 \\ \|\mathbf{d}_i\|^2 \leq 1 & i = 4, \dots, K \end{array} \right\}$$

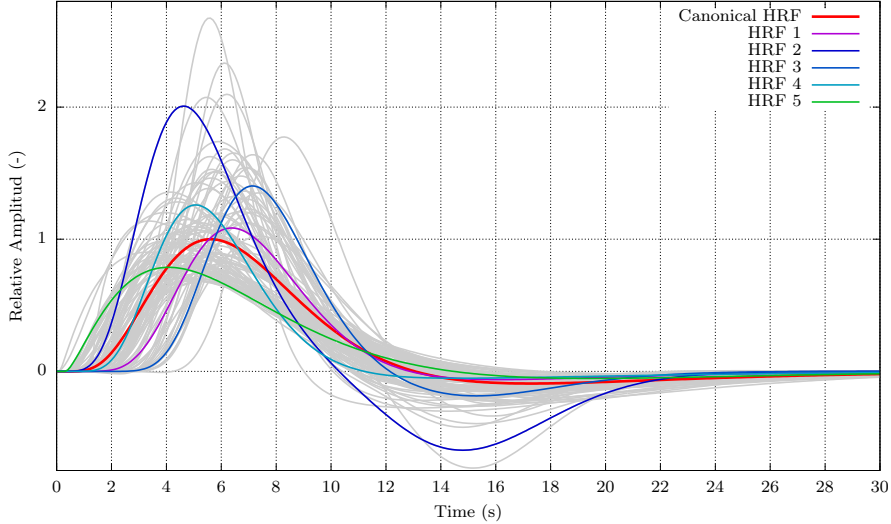


Figure 4: Representation of the 100 HRFs (grey) that were randomly generated from the two-gamma distribution model. The red HRF represents the Canonical HRF and the colored HRFs stands for the selected miss-modeled HRFs.

where δ_i are the considered task-related time courses so, in the specific case, the sources 1, 12 and 13 are imposed as δ_1 , δ_2 and δ_3 respectively. The similarity parameter was set to $c_\delta = 0.1$, which is large enough to encapsulate the variability introduced by the considered HRFs.

With respect to the sparsity constraint, the sparsity level of the task-related time courses has to be explicitly set because they are now used in the dictionary constraint, \mathfrak{D}_δ . This requirement is not essentially restrictive since the task-related sources usually correspond to functional brain networks that are depicted in brain atlases, so the specialist can have a good indication regarding to the spatial area that these networks occupy on an average brain. More importantly, the proposed method is relatively insensitive in the mis-tuning of the sources sparsity. In order to demonstrate this 3 independent source-sparsity configurations are tested, which are indicated in Table 3 as (\mathbf{I}_1) , (\mathbf{I}_2) and (\mathbf{I}_3) .

For simplicity, the task-related sources are the first three shown in the Table 3, whereas the sparsity levels of the rest of the sources is shown in descending order. As before, the sparsity level of the non task-related time sources need not be explicitly set in an one-to-one bases. Observe that configuration (\mathbf{I}_1) is closer to the true one whereas (\mathbf{I}_3) is a grossly tuned sparsity level configuration having large discrepancies from the true sparsity levels of both the task-related and the non task-related time sources. Configuration (\mathbf{I}_2) is somewhere in between.

In contrast to the proposed method, the SDL requires to tune a single regularization parameter, λ , however as it will be seen in practice is rather impossible for this single parameter to be tuned effectively since: a) the performance achieved it is very sensitive to the value of this parameter and b) it does not

Levels of Sparsity

True	Imposed		
	(\mathbf{l}_1)	(\mathbf{l}_2)	(\mathbf{l}_3)
95.28	95	95	75
91.60	90	90	85
91.53	90	80	85
97.07	97	94	90
95.53	95	93	90
95.33	95	92	90
94.57	93	91	90
94.51	92	90	90
93.30	92	89	85
92.67	92	88	85
91.82	90	87	85
88.25	88	86	85
88.07	88	85	85
86.14	85	80	80
85.51	85	75	75
77.38	77	70	75
71.95	70	65	60
71.84	70	60	20
1.99	2	0	5
1.00	0	0	2
1.00	0	0	1

Table 3: Comparison between the different implemented levels of sparsity

bearing a concise physical meaning could serve as guide for its tuning. Moreover, since in practical scenarios we do not know the true solution, tuning via cross-validation arguments are pointless. In order to study the λ mis-tune tolerance that SDL exhibits, four scenarios were tested: first, λ was set equal to the value that leads to the best estimate of the three task-related sources when the canonical HRF was imposed. In our synthetic example, since we know the true solution, this λ value can be empirically found through cross-validation. It turned out to be $\lambda_1 = 0.0008$. Then, three other values were tested, namely $\lambda_2 = 0.00008$, $\lambda_3 = 0.008$ and $\lambda_4 = 0.0000008$.

The performance results corresponding to the 5 mis-modeled HRFs as well as the true canonical HRF are shown in Fig. (4), where the number of sources has been set equal to the correct one ($K = 21$), the level of Rician noise corresponds to $\text{SNR} = 15$ and all the shown performance curves represent the ensemble average of the results obtained from 100 independent noise realizations. Moreover, the left, mid and right subfigures correspond to the average performance of the three task-related sources, the brain-like sources and all the sources, respectively. The performance of AwDL is denoted with filled circled curves and that of SDL with open squared curves.

With respect to the proposed method performance, three points are worthy

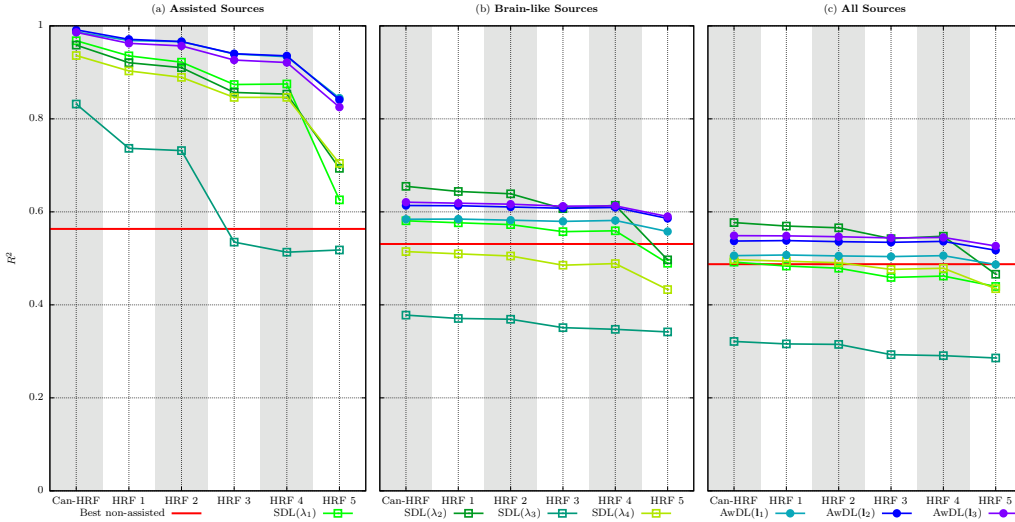


Figure 5: Experiment 2: Analysis of the different performance of for the different methods against the miss-modeling of the HRFs

to be stressed: first, it performs always better compared to the performance that is obtained without task-related course assistance, depicted with a straight red curve. More specifically, this latter curve represents the best performance achieved in experiment 1. Second, in all the sparsity configurations, the performance obtained for the assisted curves is remarkably stable. Third, the best performance in the average of brain-only sources as well as of all the sources is not achieved by the true sparsity configuration (i.e. the (I_1)). It appears that the algorithm is benefited by an under-determination of the sparsity levels. Moreover, the performance corresponding to the ‘relaxed’ sparsity level configurations (I_2) and (I_3) is essentially coincident. This is a manifestation of the robustness and the tolerance of AwDL with respect to the imposed sparsity levels.

In contrast to AwDL, SDL exhibits a rather erratic behavior for different λ values. Although for $\lambda = 0.0008$ appears to perform in the all-brain and all-sources cases somewhat better than the proposed algorithm, this performance was obtained through intensive fine-tuning and it cannot be secured in practice. Moreover, it is not guaranteed that SDL tends to perform better with relatively small λ values. The best performing value appears to be highly problem-specific and depends on the overall sparsity of the sources, the number of sources that can be simultaneously manifested in each voxel and even, in a lessen degree, on the noise level.

With respect to the robustness in HRF mis-modeling, AwDL appears much more tolerant compared to SDL, something that can be observed in the relative performance degradation caused in the mis-matched HRFs. SDL tends to degrade more than AwDL. This should be expected since SDL keeps the imposed

time-courses fixed, whereas AwDL allow them to get improved with in the limits of the corresponding constraint.

Finally, a last but important point, is the fact that SDL is computationally much more complex compared to AwDL. Detailed computational complexity analysis will be shown in a next version of the current paper.

5. Conclusions

This paper presents a new Dictionary Learning method that includes external information in a natural way via two novel convex constraints: i) a sparsity constraint based on the weighted ℓ_1 -norm, which incorporates the true level of sparsity of the spatial maps in a source by source basis and ii) a similarity constraint over the dictionary, which integrates external information from the experimental scheme.

On the one hand, the proposed similarity constraint constitutes a more natural alternative to the standard ℓ_1 -norm regularization; avoiding the implementation of regularization parameters, which need to be optimized, sometimes, following cross-validation arguments that have no practical meaning in practice.

On the other hand, the implementation of the task-related time courses from the experimental paradigm enhances the performance of all the methods. However, the newly proposed constraint exhibits more tolerance against miss-modeling of the HRF, offering a more robust alternative compared with more restrictive methods.

Extensive simulations over realistic synthetic data sets show that these two new constraints jointly cooperate, exhibiting a more discriminative power than more conventional approaches, avoiding some of the major drawbacks of the DL methods.

Bibliography

References

- [1] R. A. Poldrack, J. A. Mumford, T. E. Nichols, Handbook of functional MRI data analysis, Cambridge University Press, 2011.
- [2] Sergios Theodoridis, Machine Learning: A Bayesian and Optimization Perspective, Academic Press, 2015.
- [3] A. Protopapas, E. Orfanidou, J. S. H. Taylor, E. Karavasilis, E. C. Kapnoula, G. Panagiotaropoulou, G. Velonakis, L. S. Poulou, N. Smyrnis, D. Kelekis, Evaluating cognitive models of visual word recognition using fMRI: effects of lexical and sublexical variables, *Neuroimage* 128 (2016) 328–341.
- [4] M. G. Bright, K. Murphy, Is fMRI noise really noise? resting state nuisance regressors remove variance with network structure 114 (2015) 158–169.

- [5] E. Amaro, G. J. Barker, Study design in fMRI: basic principles 60 (3) (2006) 220–232.
- [6] F. I. Karahanoglu, C. Caballero-Gaudes, F. Lazeyras, D. Van De Ville, Total activation: fMRI deconvolution through spatio-temporal regularization, *Neuroimage* 73 (2013) 121–134.
- [7] W. D. Penny, K. J. Friston, J. T. Ashburner, S. J. Kiebel, T. E. Nichols, *Statistical parametric mapping: the analysis of functional brain images*, Academic press, 2011.
- [8] K. Friston et al., *Statistical Parametric Mapping (SPM)* (1999). URL <http://www.fil.ion.ucl.ac.uk/spm/>
- [9] G. K. Aguirre, E. Zarahn, M. D’esposito, The variability of human, BOLD hemodynamic responses 8 (4) (1998) 360–369.
- [10] A. Protopapas, E. Orfanidou, J. S. H. Taylor, E. Karavasilis, E. C. Kapnoula, G. Panagiotaropoulou, G. Velonakis, L. S. Poulou, N. Smyrnis, D. Kelekis, Evaluating cognitive models of visual word recognition using fMRI: effects of lexical and sublexical variables, *Neuroimage* 128 (2016) 328–341.
- [11] Vince D. Calhoun and Tülay Adalı, Multisubject independent component analysis of fMRI: A decade of intrinsic networks, default mode, and neurodiagnostic discovery, *IEEE Reviews in Biomedical Engineering* 5 (2012) 60–73.
- [12] W. Du, Y. Levin-Schwartz, G.-S. Fu, S. Ma, V. D. Calhoun, T. Adalı, The role of diversity in complex ICA algorithms for fMRI analysis, *Journal of Neuroscience Methods* 264 (2016) 129–135.
- [13] I. Daubechies, E. Roussos, S. Takerkart, M. Benharrosh, C. Golden, K. D’ardenne, W. Richter, J. D. Cohen, J. Haxby, Independent component analysis for brain fMRI does not select for independence 106 (26) (2009) 10415–10422.
- [14] V. D. Calhoun, V. K. Potluru, R. Phlypo, R. F. Silva, B. A. Pearlmutter, A. Caprihan, S. M. Plis, T. Adalı, Independent component analysis for brain fMRI does indeed select for maximal independence 8 (8) (2013) e73309.
- [15] Y.-B. Lee, J. Lee, S. Tak, K. Lee, D. L. Na, S. W. Seo, Y. Jeong, J. C. Ye, A. D. N. Initiative, Sparse SPM: Group sparse-dictionary learning in SPM framework for resting-state functional connectivity MRI analysis 125 (2016) 1032–1045.
- [16] Yannis Kopsinis et al., fmri unmixing via properly adjusted dictionary learning, in: *Signal Processing Conference (EUSIPCO), 2014 Proceedings of the 22nd European, IEEE, 2014*, pp. 2075–2079.

- [17] G. Zhang, Z. Jiang, L. S. Davis, Online semi-supervised discriminative dictionary learning for sparse representation, in: Asian Conference on Computer Vision, Springer, 2012, pp. 259–273.
- [18] M. M. Moreno, Y. Kopsinis, E. Kofidis, C. Chatzichristos, S. Theodoridis, Assisted dictionary learning for fMRI data analysis, in: Acoustics, Speech and Signal Processing (ICASSP), 2017 IEEE International Conference on, IEEE, 2017, pp. 806–810.
- [19] Jagath Rajapakse and Wei Lu, Extracting task-related components in functional mri, Submitted to ICA 2001 1 (2001) 120.
- [20] V. D. Calhoun, T. Adali, M. C. Stevens, K. A. Kiehl, J. J. Pekar, Semi-blind ICA of fMRI: A method for utilizing hypothesis-derived time courses in a spatial ICA analysis 25 (2) 527–538.
- [21] S. Zhao, J. Han, J. Lv, X. Jiang, X. Hu, Y. Zhao, B. Ge, L. Guo, T. Liu, Supervised dictionary learning for inferring concurrent brain networks 34 (10) (2015) 2036–2045.
- [22] W.-K. Ma, J. M. Bioucas-Dias, T.-H. Chan, N. Gillis, P. Gader, A. J. Plaza, A. Ambikapathi, C.-Y. Chi, A signal processing perspective on hyperspectral unmixing: Insights from remote sensing 31 (1) 67–81.
- [23] R. Salvador, J. Suckling, M. R. Coleman, J. D. Pickard, D. Menon, E. D. Bullmore, Neurophysiological architecture of functional magnetic resonance images of human brain, Cerebral cortex 15 (9) (2005) 1332–1342.
- [24] B. Murphy, P. Talukdar, T. Mitchell, Learning effective and interpretable semantic models using non-negative sparse embedding, Proceedings of COLING 2012 (2012) 1933–1950.
- [25] M. Yaghoobi, T. Blumensath, M. E. Davies, Dictionary learning for sparse approximations with the majorization method, IEEE Transactions on Signal Processing 57 (6) (2009) 2178–2191.
- [26] E. J. Candes, M. B. Wakin, S. P. Boyd, Enhancing sparsity by reweighted ℓ_1 minimization, Journal of Fourier analysis and applications 14 (5) (2008) 877–905.
- [27] Y. Kopsinis, H. Georgiou, S. Theodoridis, fMRI unmixing via properly adjusted dictionary learning (2014) 2075–2079.
- [28] G. I. Allen, Sparse and functional principal components analysis.
- [29] Y. Sun, P. Babu, D. P. Palomar, Majorization-minimization algorithms in signal processing, communications, and machine learning 65 (3) (2017) 794–816.

- [30] M. Razaviyayn, M. Hong, Z.-Q. Luo, A unified convergence analysis of block successive minimization methods for nonsmooth optimization 23 (2) (2013) 1126–1153.
- [31] V. Abrol, P. Sharma, S. F. Roohi, A. K. Sao, A. A. Kassim, Fast and robust fMRI unmixing using hierarchical dictionary learning, in: 2016 IEEE International Conference on Image Processing (ICIP), 2016, pp. 714–718.
- [32] J. F. Cardoso, A. Souloumiac, Blind beamforming for non-gaussian signals, IEE Proceedings F (Radar and Signal Processing) 140 (6) (1993) 362–370.
- [33] A. M. Bronstein, M. M. Bronstein, M. Zibulevsky, Y. Y. Zeevi, Sparse ICA for blind separation of transmitted and reflected images, International Journal of Imaging Systems and Technology 15 (1) (2005) 84–91.
- [34] Z. Boukouvalas, Y. Levin-Schwartz, V. D. Calhoun, T. Adalı, Sparsity and independence: Balancing two objectives in optimization for source separation with application to fMRI analysis, Journal of the Franklin Institute.
- [35] N. Correa, T. Adalı, Y.-O. Li, V. D. Calhoun, Comparison of blind source separation algorithms for fMRI using a new Matlab toolbox: GIFT, in: Acoustics, Speech, and Signal Processing, 2005. Proceedings.(ICASSP’05). IEEE International Conference on, Vol. 5, IEEE, 2005, pp. v–401.
- [36] E. B. Erhardt, E. A. Allen, Y. Wei, T. Eichele, V. D. Calhoun, SimTB, a simulation toolbox for fMRI data under a model of spatiotemporal separability, Neuroimage 59 (4) (2012) 4160–4167.
- [37] E. A. Allen, E. B. Erhardt, Y. Wei, T. Eichele, V. D. Calhoun, Capturing inter-subject variability with group independent component analysis of fMRI data: a simulation study, Neuroimage 59 (4) (2012) 4141–4159.
- [38] E. Castro, D. Hjelm, S. Plis, L. Dinh, J. Turner, V. Calhoun, Deep independence network analysis of structural brain imaging: A simulation study, in: Machine Learning for Signal Processing (MLSP), 2015 IEEE 25th International Workshop on, IEEE, 2015, pp. 1–6.
- [39] H. Gudbjartsson, S. Patz, The Rician distribution of noisy MRI data, Magnetic resonance in medicine 34 (6) (1995) 910–914.
- [40] M. Welvaert, Y. Rosseel, On the definition of signal-to-noise ratio and contrast-to-noise ratio for fmri data, PloS one 8 (11) (2013) e77089.
- [41] J. Mairal, F. Bach, J. Ponce, G. Sapiro, Online learning for matrix factorization and sparse coding, The Journal of Machine Learning Research 11 (2010) 19–60.
- [42] D. A. Handwerker, J. M. Ollinger, M. D’Esposito, Variation of BOLD hemodynamic responses across subjects and brain regions and their effects on statistical analyses, Neuroimage 21 (4) (2004) 1639–1651.